PNNL-33060

14 MeV Irradiation and Analysis of a 93% ^{239}Pu Target

Preparation for F2019 FY22 Pu Campaign

July 2022

Nic E. Uhnak, Morgan M. Haney, Larry Greenwood, Bruce Pierson, Truc Trang-Le, Dana Byram, Bruce McNamara, James Bowen, William Munley, Connor Hilton, Judah Friese, Lori Metz

U.S. DEPARTMENT OF ENERGY

Prepared for the U.S. Department of Energy under Contract DE-AC05-76RL01830

DISCLAIMER

PACIFIC NORTHWEST NATIONAL LABORATORY
operated by
BATTELLE
for the
UNITED STATES DEPARTMENT OF ENERGY
under Contract DE-AC05-76RL01830

Printed in the United States of America

Available to DOE and DOE contractors from the
Office of Scientific and Technical Information,
P.O. Box 62, Oak Ridge, TN 37831-0062;
ph: (865) 576-8401
fax: (865) 576-5728
email: reports@adonis.osti.gov

Available to the public from the National Technical Information Service
5301 Shawnee Rd., Alexandria, VA 22312
ph: (800) 553-NTIS (6847)
email: orders@ntis.gov <https://www.ntis.gov/about>
Online ordering: http://www.ntis.gov

PNNL-33060

14 MeV Irradiation and Analysis of 93% 239Pu Target in Preparation for F2019 FY22 Pu Campaign

Preparation for F2019 FY22 Pu Campaign

July 2022

Nic E. Uhnak, Morgan M. Haney, Larry Greenwood, Bruce Pierson, Truc Trang-Le, Dana Byram, Bruce McNamara, James Bowen, William Munley, Connor Hilton, Judah Friese, Lori Metz

Prepared for
the U.S. Department of Energy
under Contract DE-AC05-76RL01830

Pacific Northwest National Laboratory
Richland, Washington 99354

Summary

In this work, we present the irradiation of a 93% ^{239}Pu with 14 MeV neutrons and subsequent analysis of the fission and activation products. The fully assembled target, a Pu metal bead encapsulated in Al, further encapsulated in welded stainless steel, was analyzed 22 times over more than 100 days using gamma emission analysis (GEA). Using the results from these analyses, R-value and fission yields for fission products were determined. To prepare for the FY22 Pu irradiation using the GODIVA critical assembly at NCERC, the irradiated Pu target was disassembled, dissolved, and separated using chemistry provided by LANL collaborators. This chemical separation was intended to remove the Pu from solution with little to no effect on the remaining elements. The chemistry was assessed to try to determine possible routes of fractionation of the sample and the fission products. The separation process used was successful for the bulk of the analyzed fission and activation products, as well as the added radiotracers. Issues such as Np following Pu in the separation were likely caused by a forced break during processing. The final dissolved solution and separated fractions were analyzed by GEA looking at the remaining fission, activation and radiotracers and thermal ionization mass spectrometry analysis looking at the Pu isotopics.

Acknowledgments

Leah Arrigo's work in FY16 provided the foundation and the target for this work. This was made possible with the assistance of Morgan Haney, James Bowen, Trey Munley for the irradiation. Analysis of gamma emissions were provided by Bruce Pierson and Larry Greenwood. Gamma analysis assistance was provided by Truc Trang-Le and Dana Byram. TIMS analysis was provided by Connor Hilton. Chemical oversight for fissionable material was provided by Bruce McNamara.

Acronyms and Abbreviations

AC	Anti-Compton / Compton Suppression
CFY	Cumulative Fission Yield
cpm	Counts Per Minute
D-T	Deuterium Tritium
EOB	End of Bombardment
GABY	Gamma-Alpha-Beta-Gamma
GEA	Gamma Energy Analysis or Gamma Emission Analysis
ICP-OES	Inductively Coupled Plasma Optical Emission Spectroscopy
ICP-MS	Inductively Coupled Plasma Mass Spectrometry
in	Inches
KPA	Kinetic Phosphoresce Analysis
LANL	Los Alamos National Laboratory
MCNP	Monte Carlo N-Particle
MeV	Mega Electronvolt
mg	Milligram
NCERC	National Criticality Experiments Research Center
PNNL	Pacific Northwest National Laboratory
PYFP	Peak Yield Fission Products
RSD	Relative Standard Deviation
t-cal	Thermal Calibrations
TIMS	Thermal Ionization Mass Spectrometry

Contents

Figures

Tables

1.0 Introduction

Fission product yields and data are integral to the fundamental understanding of the fission process and feed directly into the nuclear forensics and nuclear physics models. The stronger the foundation of the nuclear data is, whether that is the uncertainty associated with a decay path or the cumulative fission yield of a specific fission product, the stronger the conclusions that can be made from the models using these data.

Within the F2019 “Integral Measurements of Independent and Cumulative Fission Product Yields,” joint project (LA19-ML-Integral_Fission_Product_Yield-NDD3Ad), there is an effort to confirm, validate or improve nuclear data, specifically fission yields. A campaign of consistent and repeated irradiations of various actinide targets irradiated at using a variety of neutron sources and experimental processes for each of the actinide’s targets is the primary means of these investigations. Multiparameter models used in support of nuclear forensic attribution are one of the primary users of these validated and improved data.

The measured fission product R-values (fission yields relative to ^{99}Mo), absolute and relative fission yields were determined for a 93% ^{239}Pu macro-target and are presented below for gamma analysis of the full target, as well as limited fission product yields from the dissolved target. This irradiation served a dual purpose of providing the material to assess the potential chemistry planned for an April irradiation joint Pacific Northwest National Laboratory (PNNL) Las Alamos National Laboratory (LANL) campaign, irradiating Pu on the Godiva critical assembly at National Criticality Experiments Research Center (NCERC).

This report summarizes a comparison between PNNL and literature values. Included in these comparisons were actinides including ^{238}Pu, ^{240}Am, and the fission products ^{89}Sr, ^{91}Y, $^{95/97}$Zr, ^{99}Mo, ^{111}Ag, $^{115/115m}$Cd, $^{136/137}$Cs, ^{140}Ba, $^{141/143/144}$Ce, ^{147}Nd, ^{153}Sm, ^{156}Eu, and ^{161}Tb, which provided total atoms as well as the R-values from the full target assembly.

2.0 Target Preparation and Irradiation

The target was assembled in FY16 according to process outlined in PNNL-30625 (Arrigo 2020) and has been stored in a safe location until August of FY21. In accordance with PNNL-30625 the nomenclature of the Pu target will be retained; the Pu target will be referred to as Pu-3 for the full assembly. The elemental composition as determined by LANL, when the Pu material was shipped is included in Table 2-1.

Table 2-1. Elemental composition of 93% Pu target material given in the historical documentation

Element or Isotope	Reference Alloy #2	Minimum Detection Limit	Element or Isotope	Reference Alloy #2	Minimum Detection Limit
Al	55(2) µg/g	20	^{232}Th	Not detected	0.2
V	Not detected	2	^{233}U	Not detected	0.2
Cr	2.8(3) µg/g	1	^{234}U	1.3(9) µg/g	0.2
Mn	3.8(3) µg/g	1	^{235}U	14(3) µg/g	0.2
Fe	293(8) µg/g	5	^{237}Np	70(1) µg/g	0.2
Ni	4(1) µg/g	1	^{238}Pu, ^{238}U	0.011(3) wt%	0.001
Cu	2(1) µg/g	1	^{239}Pu	92.93(3) wt%	0.05
Ga	9727(99) µg/g	5	^{240}Pu	5.73(3) wt%	0.001
Y	14(5) µg/g	0.2	^{241}Pu, ^{241}Am	0.263(1) wt%	0.0001
Ta	37(13) µg/g	0.2	^{242}Pu	0.0304(2) wt%	0.00005
W	119(41) µg/g	0.2			

The gamma emission analysis (GEA) of the target is shown in Table 2-2, comparing the 2016 and 2021 analysis. There is a difference in the mass determined by GEA of the ^{239}Pu, with about a 20% difference between the two analyses. This difference is likely due to the attenuation corrections applied to the in the five years between analysis. In FY 21 the gamma emission of ^{238}Pu at 152.7 keV was determined and included in the pre analysis of the target prior to irradiation.

Table 2-2. Activity, masses, and fractions of Pu and Am isotopes in Pu-3 target.

	2016			**2021**		
Sample ID	67655-24-Pu3			67655-24-Pu3		
Assay Date	10/5/2016			9/8/2021		
	Bq/sample ± 1σ%	**Wt (g)**	**% total**	**Bq/sample ± 1σ%**	**Wt (g)**	**% total**
^{238}Pu	N/A		N/A	1.24×10^{7} ± 37%	1.96×10^{-5}	9.0×10^{-3}
^{239}Pu	5.46×10^{8} ± 2%	0.238	93.3	4.67×10^{8} ± 2%	0.203	94.0
^{240}Pu	1.41×10^{8} ± 7%	1.58×10^{-2}	6.20	1.06×10^{8} ± 14%	1.26×10^{-2}	5.83
^{241}Pu	6.57×10^{8} ± 4%	1.72×10^{-4}	0.068	4.51×10^{8} ± 8%	1.18×10^{-4}	0.055
^{241}Am	4.64×10^{7} ± 12%	3.66×10^{-4}	0.144	4.53×10^{7} ± 5%	3.51×10^{-4}	0.162
Total Pu/Am		0.255			0.216	

A diagram of the full target assembly, including a fluence monitor pack, is shown in Figure 2-1. The differences between the width of the monitor foil stack and Pu-3 target is exaggerated. There was little or no difference between the diameters of the full target assembly. For the small

portion of monitor stack that extended beyond the diameter of the Pu-3 target, there is little to no difference between the neutrons moving through the stainless-steel, aluminum and Pu layers due to low cross sections particularly at 14 MeV. Table 2-3 shows the dimensions and masses of the monitor foils irradiated and their respective order.

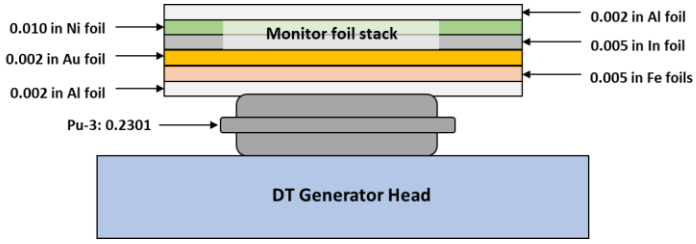

Figure 2-1. Pu irradiation target assembly and fluence monitor package.

Table 2-3. Target foils dimensions and masses

Foils in order (top to bottom)	Foil ID	Number of foils	Thickness	Weight (mg)
Al	F	1	0.002"	16.413
Ni	J	1	0.010"	278.0
In	I	1	0.005"	125.018
Au	A	1	0.002"	110.333
Fe	No ID	1	0.050"	1.2726
Al	A	1	0.002"	16.292
Pu in SS		1	0.1358"	
Front Al Foil	E	1	0.002"	16.378

Materials used
Al - Shieldwerx, Lot # SWX-505B
Fe - Shieldwerx, Lot # SWX-515
Au - Reactor Experiments Inc, Lot # 521
In - Shieldwerx, Lot # SWX-501
Ni - Shieldwerx, Lot # SWX-513A

The irradiation took place starting on September 10, 2021 and proceeded for 24 hours. An image showing the attachment of the full target assembly to the neutron generator head is shown in Figure 2-2. The disassembled full target is shown in Figure 2-3, showing both the Pu-3 target and the fluence monitor stack. Once disassembled the Pu-3 target was taken to a high purity germanium detector (HPGe) for immediate analysis by GEA, though the activity proved to be too great for this instrument due to the Al activation products. The target was moved to the track detector in the Radiological Processing Laboratory (RPL) for analysis.

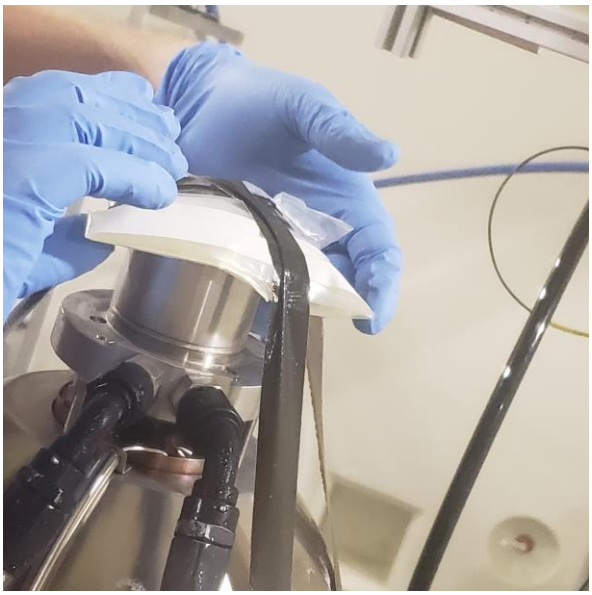

Figure 2-2. Pu-3 full target assembly and fluence monitor stack being attached to the neutron generator.

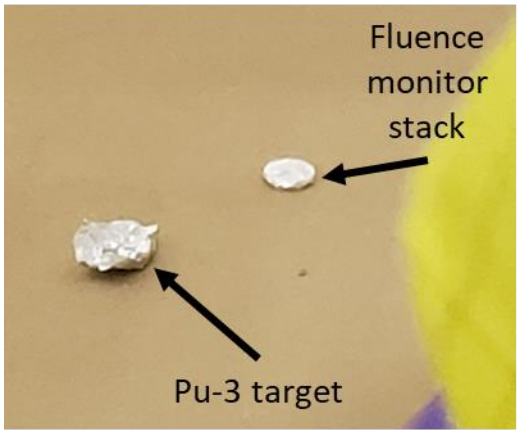

Figure 2-3. Disassembled full target assembly. The Pu-3 target wrapped in Al foil is on the left and. The fluence monitor stack is on the right.

3.0 Analysis

Once disassembled, the Pu-3 target was taken to the RPL track detector (T-detector) (as shown in Figure 3-1) and analyzed 22 times. The dates, times and durations for those analyses are shown in Table 3-1. The analysis distance was held constants for all analyses and was based on the initial efforts to minimize dead time for the first count. Processing of the GEA analysis results were processed using Genie 2k. All nuclear data was obtained from either England, or from Soperra.

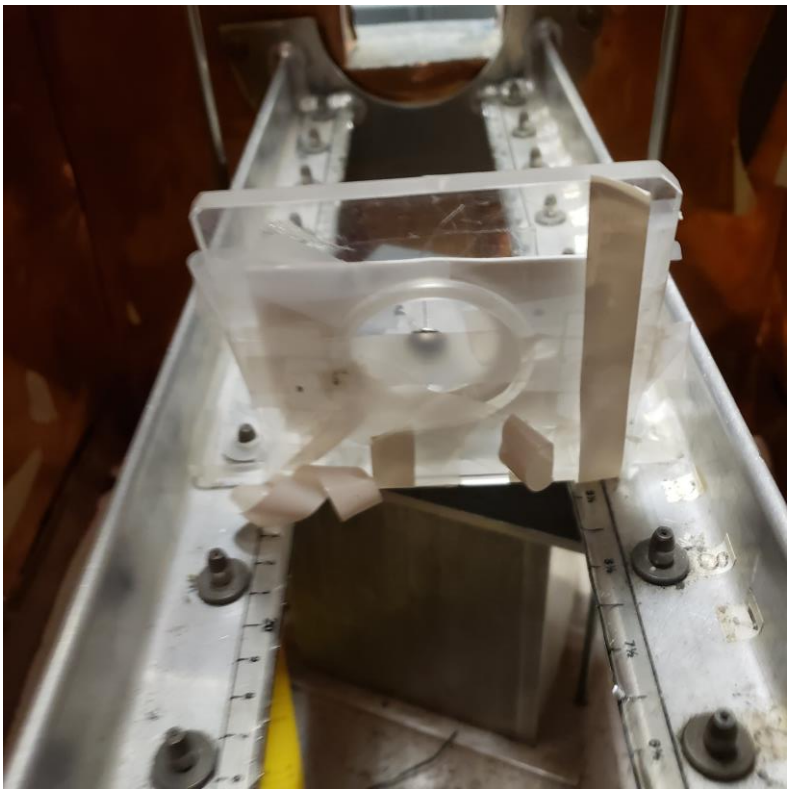

Figure 3-1. Pu-3 within the RPL track detector.

Table 3-1. Analysis dates, times, and duration of analyses of the Pu-3 target. Times are reported in Cordinated Universal Time (UTC).

Count number	Analysis Date	Analysis Duration (s)
1	9/11/2021 18:45	86400.0
2	9/12/2021 20:31	39681.1
3	9/13/2021 14:54	70663.7
4	9/15/2021 8:02	84223.9
5	9/16/2021 11:09	86400.0
6	9/20/2021 9:17	74763.9
7	9/21/2021 8:10	80241.4
8	9/24/2021 7:38	86400.0

9	9/29/2021 15:17	65892.3
10	9/30/2021 10:23	86400.0
11	10/6/2021 13:46	69462.0
12	10/13/2021 7:56	84419.6
13	10/19/2021 15:01	86400.0
14	10/28/2021 7:36	86400.0
15	11/3/2021 11:05	86400.0
16	11/10/2021 12:59	86400.0
17	11/23/2021 13:35	86400.0
18	11/30/2021 13:11	86400.0
19	12/7/2021 10:05	71628.3
20	12/15/2021 14:12	86400.0
21	12/20/2021 10:54	86400.0
22	1/5/2022 12:20	86400.0

The activities over all counts were decay corrected to the end of bombardment, averaged and the respective uncertainties were propagated. The atoms/g obtained from all detected fission and activation product stemming from the Pu-3 target are reported in Table 6-1. Table 6-1 does not include the fission products or activation products arising from the stainless steel or aluminum activation products. Discussion of specific fission or activation products as well as the activation of the stainless-steel is included in Section 6.0.

4.0 R-value calculation

4.1.1 R-value calculation – PNNL

The analytical results were used to calculate the R-value for each fission product; the method for calculating the R-value is shown in Equation 1. PNNL has a running historical r-value (r_{hist}) for each isotope based on the results from the last 5 thermal calibration (t-cal) exercises where available. A t-cal exercise involves the thermal irradiation of ^{235}U followed by separation and radiometric analysis. The historical r-value replaces the ENDF/B-VII.I CFY in the R-value calculation. The historical r-values used in the R-value calculation are shown in Table 4-1. A few isotopes including ^{91}Sr, ^{93}Y, ^{112}Ag, and ^{156}Sm are not measured in t-cal solutions and do not have r_{hist} values; in these cases, the applicable ENDF/B-VII.I CFY values have been used.

Equation 1. **R-value calculation for measurements at PNNL**

$$R = \frac{\left(\frac{N_X}{N_{Mo99}}\right)_{Measured}}{\left(\frac{N_x}{N_{Mo99}}\right)_{U235\ Thermal}} = \frac{\left(\frac{N_X}{N_{Mo99}}\right)_{Measured}}{\left(\frac{CFY_x}{CFY_{Mo99}}\right)_{U235\ Thermal}} = \frac{\left(\frac{N_X}{N_{Mo99}}\right)_{Measured}}{r_{hist}}$$

N_X – atoms of isotope X per gram of A solution
N_{Mo99} – atoms of ^{99}Mo per gram of A solution
CFY_X – CFY for isotope X for ^{235}U thermal fission
CFY_{Mo99} – CFY for ^{99}Mo for ^{235}U thermal fission
r_{hist} – historical r-value as determined in Equation 2

Equation 2**: Historical r-value**

$$r_{hist} = \left(\frac{N_X}{N_{Mo99}}\right)_{t-cal}$$

N_X – atoms of isotope X per gram of A solution in a t-cal sample
N_{Mo99} – atoms of ^{99}Mo per gram of A solution in a t-cal sample
t-cal – thermal calibration exercise sample

Table 4-1. PNNL historical r-values

Isotope	r_{hist}	Isotope	r_{hist}
^{89}Sr	0.793	^{136}Cs	$9.67x10^{-4}$
^{91}Sr	N/A	^{137}Cs	1.05
^{91}Y	0.939	^{140}Ba	1.05
^{93}Y	N/A	^{141}Ce	0.971
^{95}Zr	1.09	^{143}Ce	0.994
^{97}Zr	1.05	^{144}Ce	0.910
^{103}Ru	0.504	^{147}Nd	0.365
^{111}Ag	$2.80x10^{-3}$	^{153}Sm	$2.22x10^{-2}$
^{112}Ag	N/A	^{156}Sm	N/A
^{115}Cd*	$2.21x10^{-3}$	^{155}Eu	$5.37x10^{-3}$
^{115m}Cd	$7.90x10^{-5}$	^{156}Eu	$2.44x10^{-3}$
^{132}Te	0.719	^{161}Tb	$1.29x10^{-5}$

Isotope	r_{hist}	Isotope	r_{hist}

4.1.2 Fission yield Calculations

Calculations of the fission yields were conducted using two methods, the absolute fission yield shown in Equation 3, and the relative fission yield is shown in Equation 4. Examples of both methods of calculation are shown in the appendix A.2 for ^{136}Cs at fission spectrum.

$$CFY_X = \frac{Atoms_X/g}{Fissions/g}$$

Equation 3. Absolute fission yield

$$\mathrm{R} = \frac{\left(\frac{CFY_X}{CFY_{Mo99}}\right)_{fission}}{\left(\frac{\mathrm{CFY_X}}{\mathrm{CFY_{Mo99}}}\right)_{\mathrm{U235\ thermal}}}$$

Equation 4. Relative Fission yield

Rearrangement of Equation 5, the R-value used in the calculation of the relative fission yield is the average of all measured R-values.

$$\mathrm{CFY}_{Xfission} = R \times \frac{CFY_{Mo99fission} \times CFY_{Xth}}{CFY_{Mo99th}}$$

Equation 5. Reorganized relative fission yield equation

5.0 Dissolution, Separation and Analysis

The primary motivation to remove the Pu target from its stainless-steel encasement was to assess the viability of the separation proposed by collaborators at LANL for the FY22 R-value campaign that includes an irradiation of 93% ^{239}Pu by fission spectrum neutrons at NCERC. The disassembly, dissolution, and separation will be discussed in this section with post dissolution analysis discussed in detail in subsequent sections.

A glovebag from Lancs Industries was setup within a radiological fumehood. Several items were arranged in the glovebag to both open the capsule, as well as dissolve and process the Pu target. The glovebag equipment is shown in Figure 5-1, with labels showing each of the items used. A 500 mL two neck flask was used for the dissolution (2), heating during the dissolution process was provided by a heating mantle (3). To cool the condenser flask (4), a water-cooling pump was used with tubing going in and out of the glovebag (5). During dissolution of Pu a stream of Ar (1) was used to push the vapor into the condensing flask (4) with any vapor pushed out further (6) to a gas drying trap filled with 50:50 mixture of CaO and Drierite (7). The gas drying trap was used to ensure that the integrity of the stainless-steel hood was maintained, capturing any water vapor, acid vapor, or potential gaseous fission products such as ^{131}I, or $^{133/135}$Xe (not expected due to $t_{1/2}$).

Figure 5-1. Glovebag setup for Pu processing.

The glovebag setup for the stainless-steel capsule removal is shown in Figure 5-2. Note that the weigh boat shown in the images was used to retain any stray pieces of stainless steel. The stainless-steel capsule was removed by carefully cutting the welds around the center bulge of the capsule (red dotted line). Once nearly all welds were removed as depicted in Figure 5-3, the capsule was squeezed along the edges, allowing the stainless-steel capsule to open and the aluminum capsule containing the Pu material to fall out. The aluminum capsule was transferred into the round bottom flask for dissolution.

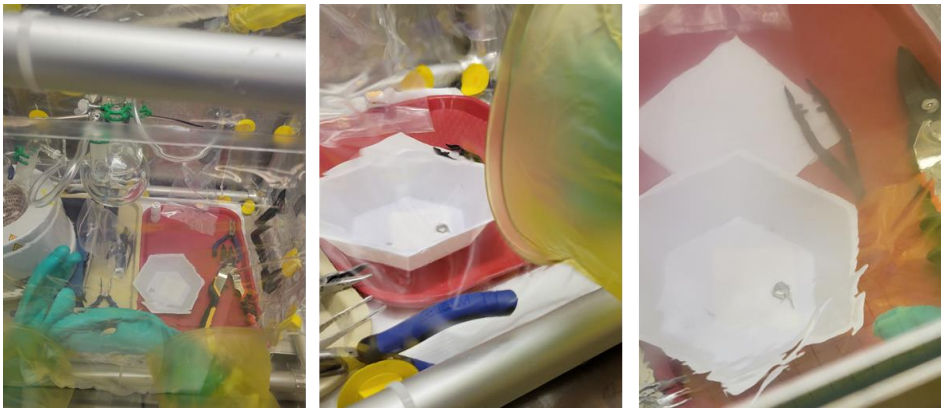

Figure 5-2. Removal of stainless steel capsule from Pu target in glovebag.

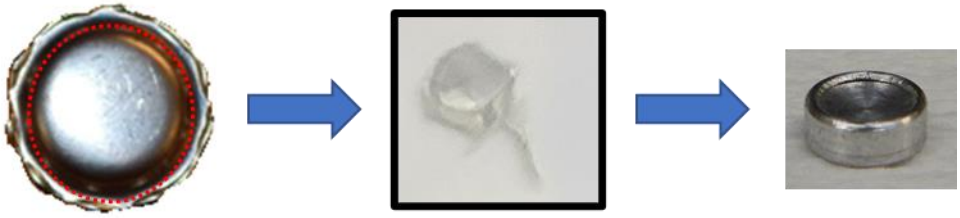

Figure 5-3. Capsule removal process, showing from left to right, the full stainless steel encapsulated target, the removal of the stainless, and finally the Al encapuslated Pu target.

The dissolution process is shown in Figure 5-4. The Pu encapsulated in Al was placed in a round bottom flask (left most picture), additions of concentrated HNO_3 and concentrated HCl were made (initial addition of 30 mL of concentrated HNO_3, 6 mL of concentrated HCl was added). The solution was heated to boiling, with a slow flow of Ar to push the vapor into the condenser. All dissolution, heating, transposing occurred in the apparatus shown in Figure 5-1. Periodic additions of 3-5 mL of concentrated HNO_3 were made to transpose the solution from mixed HNO_3/HCl to only HNO_3 and to ensure that the small black particulate (PuO_2) was dissolved fully. The solution was transposed with an addition of 10 mL of concentrated HNO_3, this was evaporated to near dryness and repeated two more times and the process was then repeated identically with 8 M HNO_3.The fourth image in Figure 5-4 shows the dissolved Pu dried to near dryness during the transposition. The final image in Figure 5-4 shows the fully dissolved Pu sample, a dark green solution.

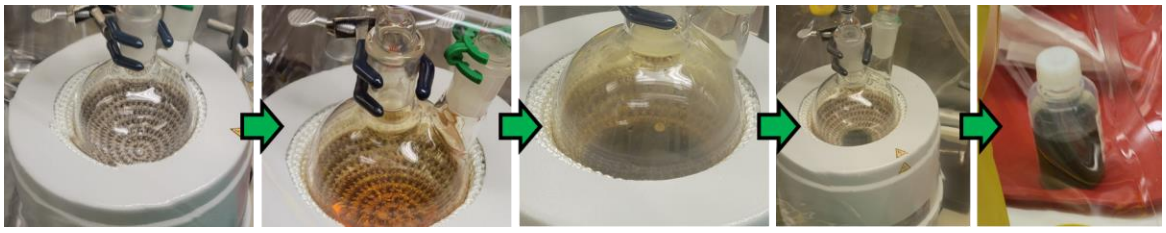

Figure 5-4. Dissolution and transposition process for Pu-3 target.

Once dissolved, the solution was removed from the glovebag and weighed on a balance. The solution was split according to the information in Table 5-1 to provide 2 replicates and an A solution for analysis by GEA. During this splitting process several radioactive yield tracers were added to the solutions. During this process a small quantity of replicate 1 was spilled, a volume adjustment was made to ensure that the concentrations of Pu, tracers and HNO_3 were similar

between the two replicates. The tracers were in two separate vials, one containing ^{110m}Ag and the other containing stable tracers, as well as ^{152}Eu, ^{109}Cd, ^{134}Cs, and ^{237}Np. Each of these solutions were transferred quantitatively with 8 M HNO_3, bringing the total final volume to ~15 mL (with roughly 2 mL spill of replicate 1). Each replicate was made to contain 40-45 mg of Pu, to mirror what would be expected from the irradiated Pu target aimed for the April FY22 Godiva irradiation F2019 joint exercise. A sample for the Gabriel (a gamma, alpha, beta, gamma coincidence) detector was also prepared though, a so-called GABY sample as labeled in Table 5-1. Although, data obtained from this detector is not expected to be completely interpreted before this report is completed. The thermal ionization mass spectroscopy (TIMS) sample was used for the confirmation of the isotopic ratios of the Pu isotopes.

Table 5-1. Masses and splits of A solutions, replicates, TIMS, and GABY samples for Pu-3 irradiation.

Sample	A solution (g)	Diluent (g)	Tracers + rinse	Diluent solution	Total Solution Mass	Dilution of A (by mass)
A solution			57.0282			
A solution GEA			12.7234			
B solution	1.2665	8.9877		Water	10.2542	8.1x
C solution	2.0422 (*B*)	9.9410		8 M HNO_3	11.9832	47.5x
D solution	0.1184 (*C*)	12.3926		8 M HNO_3	12.5109	5020x
E solution	0.1740 (*D*)	12.5393		8 M HNO_3	12.7133	$3.67x10^5$x
Replicate 1	10.6414	7.3703	3.8989	8 M HNO3	21.9106	
Replicate 2	12.6521	6.7442	4.5980	8 M HNO3	23.9943	
TIMS	0.1 mL (*C*)		N/A			
GABY	0.1 mL (*B*)			Ultima Gold AB		

Four columns containing 15 mL of AG-MP-1 anion exchange resin (50-100 mesh, chloride form) were prepared and rinsed with 60 mL of 8 M HNO_3 prior to transferring into the glovebag. The samples included two replicates, as well as, a tracer blank containing only the tracers, and a reagent blank containing only the reagents. The simple flow chart used for the Pu separation is shown in Figure 5-5. The sample replicates were loaded on their respective columns, rinsed with 8 M HNO_3 collecting this solution as the load/rinse fraction. The elution of Pu was accomplished by using 0.1 M HNO_3, eluting 45 mL (3x bed volumes) collected as Elute 1 and was repeated a second time for a second elution. A similar process was repeated with the tracer blank and reagent blank.

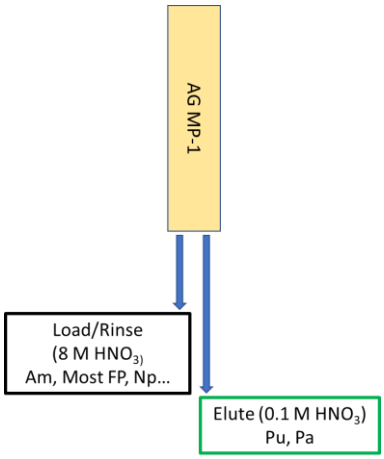

Figure 5-5. Simple Pu separation flow chart.

Plutonium in high HNO_3, more specifically Pu(IV), is a dark green color. The speciation of Pu facilitates this separation, existing as $Pu(NO_3)_6^{2-}$ in $[HNO_3] \approx 8$ M HNO_3. Evidence of this can be seen in left picture in Figure 5-6, showing a green band on top of the AG MP-1 anion exchange column. Eluting the Pu with 0.1 M HNO_3 alters the Pu speciation to $Pu(NO_3)_x^{4-x}$ (x=1-4) allowing it to be removed from the column. The Pu elution and change in speciation is shown in the right-hand picture in Figure 5-6, showing that the green band had been removed from the column.

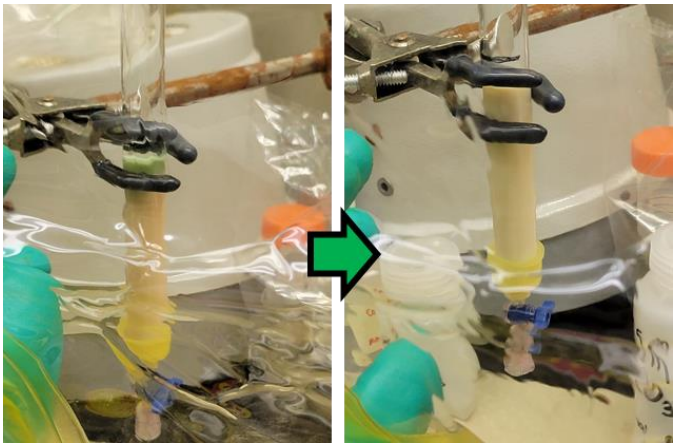

Figure 5-6. Anion exchange column loaded with Pu, before and after Pu elution with 0.1 M HNO_3.

TIMS analysis for Pu isotopic composition used a Thermo Scientific Triton *Plus* multi collector TIMS. This instrument has 10 faraday cups, allowing for simultaneous measurement of ^{238}Pu, ^{239}Pu, ^{240}Pu, ^{241}Pu, and ^{242}Pu isotopes. Samples were corrected for instrumental mass fractionation by measuring the New Brunswick Laboratory Pu standard C128 as a reference. Samples and standards were analyzed using a double rhenium filament assembly by a total evaporation method. Approximately 200 ng of Pu was consumed per analysis.

6.0 Results

6.1 Full assembled target analysis

The analysis of the full target offers a unique opportunity that the dissolved target does not, including the analysis of volatile fission products such as ^{103}Ru, radioiodine, and radioxenon. Results obtained from the 22 counts were averaged where applicable, uncertainties propagated, and are shown in Table 6-1. Also included in Table 6-1 is a comparison of the experimentally determined R-values using both the ENDF CFY, as well as r-hist compared to the ENDF calculated R-value for both ^{99}Mo and ^{140}Ba, where applicable. [Soppera] All ^{140}Ba R-values were calculated using the ENDF CFYs and did not consider the r-hist.

The experimental R-values are by and large in excellent agreement with the literature values, with ^{95}Zr, ^{97}Zr, ^{103}Ru, ^{112}Ag, ^{125}Sn, ^{127}Sb, ^{132}Te, ^{140}Ba, ^{140}La, and^{151}Pm notably being within 1σ of the literature value. Due to the prominence of the ^{241}Am gamma emissions at 59 keV the analysis of the ^{137}Cs could not be completed.

Table 6-1. Atoms/g of the Pu-3 target in the full assembly, comparison of the experimental R-value and literature R-value, presented with associated uncertainties. Experimental R-values in italics were calculated using r-hist.

	Atoms/g	±%	Exp. R_{Mo-99}	±%	Exp. R_{Ba-140}	±%	R-ENDF	±%
Sr91	8.70×10^{9}	2.3%	0.682	5.7%	0.995	4.2%	0.412	12.2%
Sr92	9.50×10^{9}	7.0%	0.569	13%	0.830	13.5%	0.469	23.6%
Y93	1.42×10^{10}	8.7%	0.68	65.1%	0.991	64.7%	0.509	90.7%
Zr95	1.61×10^{10}	0.4%	0.749	5.8%	1.09	4.3%	0.728	8.1%
Zr97	1.65×10^{10}	0.6%	0.837	5.9%	1.22	4.5%	0.852	7.5%
Nb95	2.37×10^{9}	0.7%					0.729	8.1%
Nb97	1.24×10^{9}	0.7%					0.876	7.3%
Mo99	1.94×10^{10}	1.2%	1.00	2.4%	1.40	4.3%		
Ru103	1.92×10^{10}	0.4%	1.92	5.8%	2.80	4.3%	2.09	8.1%
Rh105	2.11×10^{10}	1.3%	6.63	6.4%	9.67	5.1%	4.78	8.2%
Ag111	2.62×10^{10}	4.6%					119	10.3%
Ag112	7.05×10^{9}	1.0%	164	8.2%	239	7.2%	154	9.9%
Cd115	4.05×10^{9}	2.0%	106	8.2%	154	7.2%	133	11.3%
Sn125	3.06×10^{9}	7.8%	57.9	10.2%	84.5	9.4%	59.2	32.7%
Sb127	7.71×10^{9}	1.6%	14.9	6.9%	21.7	5.7%	14.7	8.9%
Te129	4.81×10^{11}	38.7%					5.30	16.9%
Te129m	7.05×10^{10}	2.0%					8.57	45.3%
Te131m	6.79×10^{9}	1.1%	4.99	6.9%	7.28	5.7%	3.45	23.9%
Te132	1.25×10^{10}	1.9%	0.880	5.8%	1.28	4.3%	0.830	8.1%
I131	1.68×10^{10}	0.5%			2.56	15.4%	0.727	12.2%

I132	$1.28x10^{10}$	0.4%	0.899	6.4%	1.31	64.1%	1.02	9.1%
I133	$1.81x10^{10}$	1.4%	0.819	6.4%	1.19	64.1%	0.765	90.7%
I135	$1.04x10^{10}$	1.5%	0.503	5.8%	0.733	4.3%	0.610	45.3%
Cs136	$2.79x10^{9}$	0.5%			223	64.2%	52.2	9.1%
Cs137‡	$1.25x10^{12}$	0.4%				89.2	8.2%	9.6%
Ba139	$1.72x10^{10}$	21.5%	0.814	5.3%	1.19	3.6%	0.766	12.2%
Ba140	$1.41x10^{10}$	0.7%	0.686	6.3%	1.00	5.0%	0.705	7.3%
La140	$1.4x10^{10}$	0.3%	0.68	8.0%	0.998	7.0%	0.73	8.0%
Ce141†	$4.26x10^{10}$	1.0%				3.22	4.2%	8.0%
Ce143	$1.11x10^{10}$	0.9%	0.565	5.8%	0.824	4.3%	0.594	8.1%
Nd147	$6.41x10^{9}$	7.5%	0.865	9.3%	1.26	8.4%	0.922	8.1%
Pm149	$2.74x10^{9}$	12.2%	0.769	13.5%	1.12	12.9%	1.20	23.7%
Pm151	$3.41x10^{9}$	4.9%	2.47	7.4%	3.60	6.3%	2.15	32.5%
Sm153	$1.05x10^{11}$	2.0%			294	5.9%	3.91	17.3%
Eu156	$5.18x10^{8}$	19.3%	10.6	20%	15.4	20.0%	18.5	8.9%
				†^{239}Pu gamma interference ‡ ^{241}Am gamma interference				

The data obtained from the 22 counts of the full target assembly was used to calculate the R-values, the results of which are shown in Figure 6-1. The ENDF R-values were calculated using the CFY in the ENDF.V.III.0 database. Based on these comparisons there is a high degree of agreement between the literature and experimental R-values. Only the ^{99}Mo R-values are included in Figure 6-1..

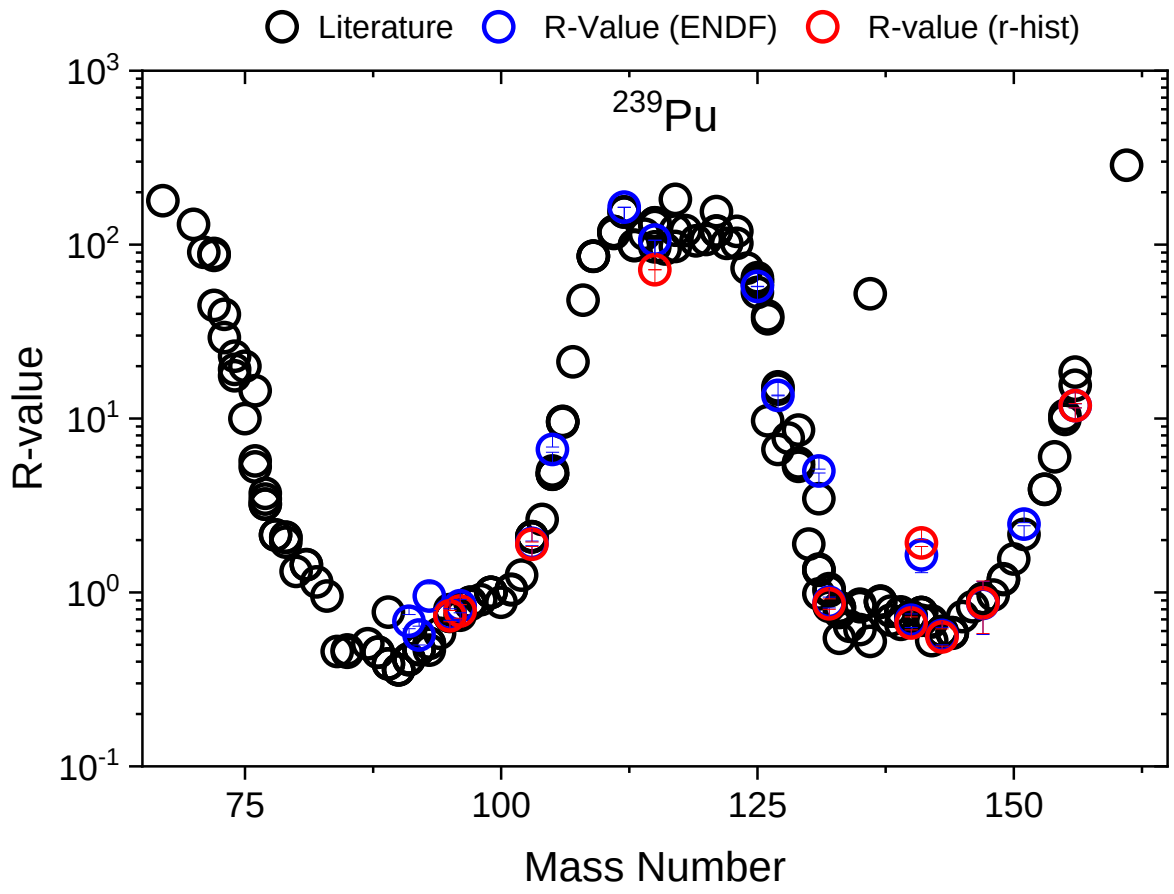

Figure 6-1. Experimentally determined R-values compared to the literature values using both the ENDF yields, or the r-hist. Uncertainties are 1σ of those values.

Using Equation 3 and Equation 5, the absolute and relative fission yields were calculated. The calculation of the number of fissions did not include the ^{99}Mo or ^{95}Zr due to the external source from stainless-steel activation. A total of 3.17x10^{11} fissions/g were determined and this value was used in the absolute fission yields values. The results are tabulated in Table 6-2, comparing the absolute, relative and literature fission yields from ENDF.V.III.0. The encapsulation allowed for the direct determination of the fission yields of iodine fission products, that are generally lost in the dissolution process of the target after irradiation. Due to the activated ^{99}Mo and ^{95}Zr from the stainless-steel capsule, a direct comparison between two other high yield fission products is included, those are ^{95}Zr, and ^{140}Ba. The overall agreement between the absolute, relative and literature fission yields is high, with some notable exceptions such ^{136}Cs, an isolated fission product with a low yield. The relative and literature values line up well, but the absolute is significantly higher, likely an indication of an interference causing an overestimation of the activity. Others such as ^{149}Pm, whose relative and absolute fission yields agree do not agree with the literature, require further investigation through more irradiations.

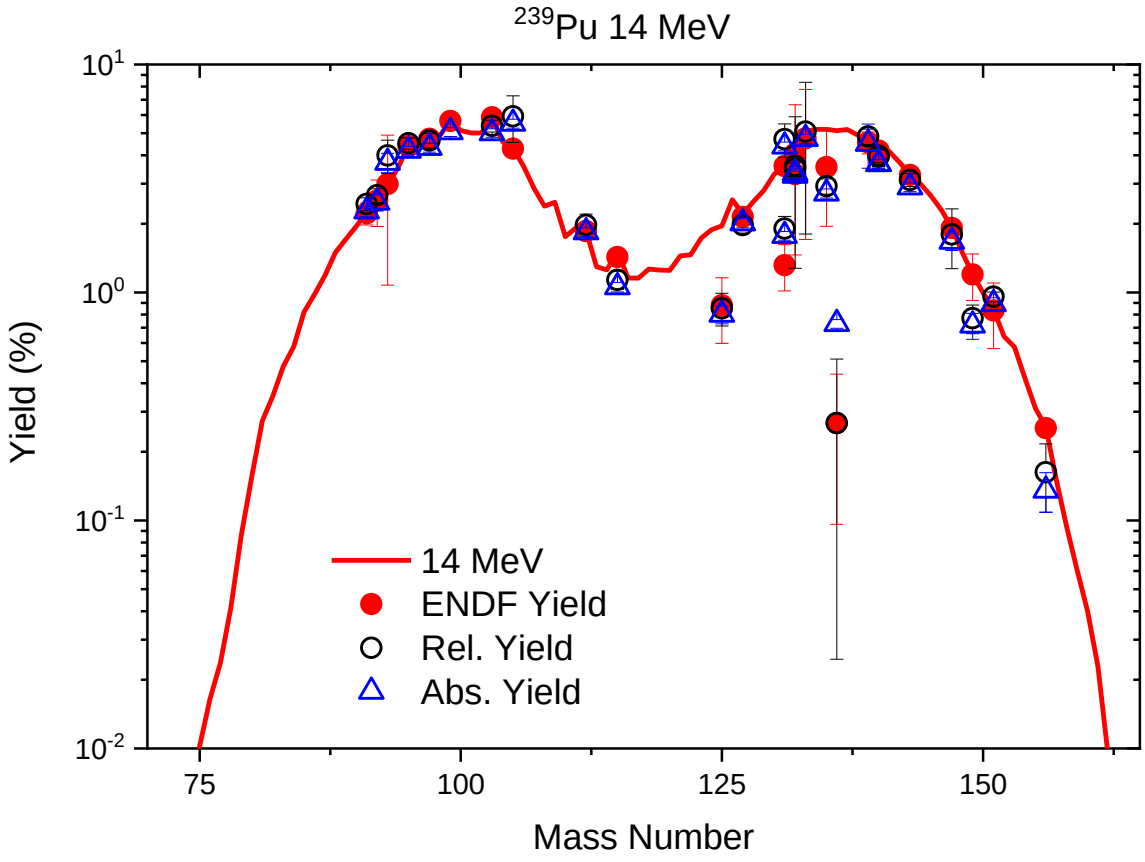

Figure 6-2. Fission yields obtained from the analysis of Pu-3 target. The line shows the CFY for a given mass number, the ● symbols show the ENDF.V.III.0 CFY with associated uncertainties (obtained from Soppera), the ○ shows the relative fission yields, the △ symbols show the absolute fission yields.

Table 6-2. Absolute and relative fission yields calculated from fully assembled irradiated Pu target.

Fission Product	Absolute Fission Yield	Relative Fission Yield ^{99}Mo	Relative Fission Yield ^{140}Ba	Relative Fission Yield ^{95}Zr	Literature Fission Yield (ENDF)
Sr91	2.74 ± 4.9%	2.44 ± 8.1%	2.51 ± 6.5%	2.38 ± 6.9%	2.22 ± 11%
Sr92	3.00 ± 8.2%	2.67 ± 8.6%	2.74 ± 14.4%	2.59 ± 14.6%	2.53 ± 23%
Y93	4.48 ± 9.7%	2.85 ± 90.8%	2.93 ± 90.8%	2.77 ± 90.8%	2.99 ± 64%
Zr95	5.06 ± 4.3%	4.51 ± 7.6%	4.63 ± 6.6%	4.38 ± 6.9%	4.38 ± 6.0%
Zr97	5.21 ± 4.3%	4.64 ± 8.9%	4.77 ± 6.7%	4.51 ± 7.1%	4.72 ± 5.0%
Mo99	6.11 ± 4.5%	6.02 ± 5.6%	5.59 ± 6.6%	5.29 ± 6.9%	5.66 ± 5.0%
Ru103	6.05 ± 4.3%	5.38 ± 7.8%	5.54 ± 6.6%	5.24 ± 7.0%	5.86 ± 6.0%
Ag112	2.22 ± 4.4%	1.98 ± 13%	2.03 ± 8.8%	1.93 ± 9.1%	1.86 ± 6.0%
Cd115	1.28 ± 4.8%	1.14 ± 10%	1.17 ± 8.8%	1.10 ± 9.1%	1.43 ± 8.0%
Sn125	0.97 ± 8.9%	0.85 ± 17%	0.88 ± 10.6%	0.84 ± 10.9%	0.88 ± 32%
Sb127	2.43 ± 4.6%	1.97 ± 9.2%	2.22 ± 7.6%	2.10 ± 7.9%	2.14 ± 6.0%

Te131m	2.14 ± 4.4%	1.91 ± 14%	1.96 ± 7.6%	1.85 ± 7.9%	1.32 ± 23%
Te132	3.93 ± 4.7%	3.49 ± 8.0%	3.60 ± 6.6%	3.40 ± 6.9%	3.30 ± 6.0%
I132	4.03 ± 4.3%	3.59 ± 64%	3.69 ± 90.8%	3.49 ± 90.8%	4.06 ± 64%
I133	5.70 ± 4.5%	5.08 ± 90.8%	5.22 ± 90.8%	4.94 ± 90.8	4.74 ± 64%
I135	3.28 ± 4.5%	2.92 ± 7.6%	3.01 ± 6.6%	2.84 ± 6.9%	3.55 ± 45%
Cs136	0.73 ± 4.3%	0.78 ± 91%	0.81 ± 90.8%	0.76 ± 90.8%	0.27 ± 64%
Ba139	5.43 ± 21.9%	4.83 ± 5.3%	4.97 ± 6.2%	4.70 ± 6.5%	4.55 ± 11%
Ba140	4.43 ± 4.4%	3.97 ± 6.2%	4.06 ± 7.1%	3.84 ± 7.4%	4.06 ± 5.0%
La140	4.42 ± 4.3%	3.94 ± 9.4%	4.05 ± 8.6%	3.83 ± 8.9%	4.19 ± 6.0
Ce143	2.90 ± 4.4%	3.11 ± 6.5%	3.38 ± 6.6%	3.03 ± 6.9%	3.28 ± 6.0%
Nd147	1.67 ± 8.7%	1.80 ± 29%	1.85 ± 9.8%	1.75 ± 10.0%	1.92 ± 6.0%
Pm149	0.72 ± 13%	0.77 ± 14%	0.79 ± 13.8%	0.75 ± 14.0%	1.20 ± 23%
Pm151	0.89 ± 6.5%	0.96 ± 4.9%	0.98 ± 8.1%	0.93 ± 8.0%	0.83 ± 32%
Eu156	0.16 ± 19.7%	0.16 ± 33%	0.15± 21%	0.14 ± 21%	0.25 ± 6.0%

The comparison of ^{140}Ba, ^{95}Zr, and ^{99}Mo relative fission yields allows for direct comparison between two fission products that had an external source and one that did not. The calculated fission yields relative to the high yield fission products largely compare well to the literature values, as well as the absolute fission yields (relative to total fissions).

6.1.1 Actinide Activation Product Analysis

The actinide activation products were determined by GEA of the full target. The results are shown in Table 6-3. The activity is shown as the average of the total number of counts and the uncertainty is the propagated uncertainty for the single sample. Several nuclear reactions produce these actinide activation products, including ^{241}Am(n,2n)^{240}Am, or ^{239}Pu(n,3n)^{237}Pu. The detection of some of the potential activation products is limited due to the nuclear reaction cross sections at 14 MeV, which are low.

Table 6-3. Actinide gamma analysis, including activation and decay products from full target assembly

Count number	^{233}Pa	^{237}U	^{237}Np	^{239}Np	^{239}Pu	^{240}Pu	^{241}Pu	^{240}Am	^{241}Am
					Bq/g				
1		$6.70\times10^{4} \pm 4\%$		$4.20\times10^{3} \pm 24\%$	$2.14\times10^{9} \pm 2\%$			380 ± 28%	$1.84\times10^{8} \pm 10\%$
2		$7.12\times10^{4} \pm 3\%$		$3.44\times10^{3} \pm 21\%$	$2.08\times10^{9} \pm 2\%$			364 ± 32%	$1.83\times10^{8} \pm 3\%$
3		$8.01\times10^{4} \pm 3\%$			$2.10\times10^{9} \pm 2\%$				$1.89\times10^{8} \pm 3\%$
4		$1.032\times10^{5} \pm 2\%$			$2.21\times10^{9} \pm 2\%$			210 ± 19%	$2.55\times10^{8} \pm 2\%$
5		$1.12\times10^{5} \pm 2\%$		$1.91\times10^{3} \pm 18\%$	$2.16\times10^{9} \pm 2\%$				$2.01\times10^{8} \pm 4\%$
6				$4.15\times10^{3} \pm 33\%$	$2.14\times10^{9} \pm 2\%$				$2.02\times10^{8} \pm 4\%$
7		$1.96\times10^{5} \pm 2\%$			$2.21\times10^{9} \pm 2\%$				$2.64\times10^{8} \pm 2\%$
8	$3.36\times10^{3} \pm 11\%$	$2.51\times10^{5} \pm 2\%$			$2.10\times10^{9} \pm 2\%$				$1.99\times10^{8} \pm 2\%$
9		$4.54\times10^{5} \pm 2\%$			$2.20\times10^{9} \pm 2\%$				$2.62\times10^{8} \pm 2\%$
10		$4.58\times10^{5} \pm 2\%$			$2.13\times10^{9} \pm 2\%$				$2.00\times10^{8} \pm 4\%$
11		$9.28\times10^{5} \pm 2\%$			$2.20\times10^{9} \pm 2\%$				$2.64\times10^{8} \pm 2\%$
12					$2.19\times10^{9} \pm 2\%$				$1.97\times10^{8} \pm 2\%$
13					$2.14\times10^{9} \pm 2\%$				$1.96\times10^{8} \pm 2\%$
14	$5.55\times10^{3} \pm 2\%$				$2.12\times10^{9} \pm 2\%$				$1.96\times10^{8} \pm 2\%$
15		$1.60\times10^{7} \pm 2\%$	$7.69\times10^{3} \pm 5\%$		$2.20\times10^{9} \pm 2\%$				$2.59\times10^{8} \pm 2\%$
16		$3.39\times10^{7} \pm 2\%$			$2.21\times10^{9} \pm 2\%$				$2.65\times10^{8} \pm 2\%$
17					$2.13\times10^{9} \pm 2\%$				$1.97\times10^{8} \pm 2\%$
18	$2.78\times10^{3} \pm 2\%$		$6.49\times10^{3} \pm 7\%$		$2.19\times10^{9} \pm 2\%$				$2.60\times10^{8} \pm 2\%$
19	$3.84\times10^{3} \pm 4\%$				$2.13\times10^{9} \pm 2\%$		$2.04\times10^{9} \pm 4\%$		$1.97\times10^{8} \pm 2\%$
20	$4.01\times10^{3} \pm 4\%$				$2.15\times10^{9} \pm 2\%$				$2.58\times10^{8} \pm 9\%$
21	$3.87\times10^{3} \pm 6\%$				$2.13\times10^{9} \pm 2\%$		$1.97\times10^{9} \pm 4\%$		$1.97\times10^{8} \pm 2\%$
22	$4.13\times10^{3} \pm 47\%$				$2.13\times10^{9} \pm 2\%$	$5.27\times10^{8} \pm 8\%$	$2.00\times10^{9} \pm 4\%$		$2.00\times10^{8} \pm 2\%$

6.2 Disassembled target analysis

6.2.1 Stainless Steel Analysis

The stainless-steel alloy used is not known, but in general stainless-steel alloys require >11% Cr, >8% Ni, ~1% C, with the balance consisting of mainly Fe. There are other elemental contributions depending on the alloy, such as Mo addition in stainless-steel 316. Confirmation of the stainless-steel alloy was conducted using a Thermo Niton XL5 handheld x-ray fluorescence spectrometer (XRF). The identified alloy, AISI stainless-steel 304, was found within the instrument's alloy library. The empty stainless-steel capsule was analyzed. Results are reported in Table 6-4, as a range from multiple measurements of the irradiated capsule as well as unused capsule. Only elements greater than 0.1% of the total composition are reported.

Based on the total mass of the stainless-steel capsule, the contribution of ^{99}Mo from neutron bombardment from the natural Mo in the capsule was determined. The mass of the stainless-steel was measured at 0.5002 g, the contribution to this mass from natural Mo is ~2 mg, and ~0.2 mg of that is ^{100}Mo. Similarly, ^{95}Zr is produced from the ^{98}Mo(n,α) reaction. Calculation of the activation product ^{99}Mo accounts for ~5-10% excess ^{99}Mo relative to the fission product Mo. A similar result is seen with ^{95}Zr. Because of this Mo excess, the relative fission yields are calculated relative to multiple peak yield fission products, including ^{140}Ba, ^{95}Zr, and ^{99}Mo.

Table 6-4. Elemental composition of stainless-steel capsule. Values are reported as a percent of the total composition. Literature values reported as a range.

Element	Measured	Literature SS-304
Fe	68-70%	69-75%
Cr	19-21%	17-20%
Ni	7-8.5%	7.8-10.5%
Mn	1.3-2.2%	0-2%
Cu	0.38-0.4%	0-0.75%
Si	0.4-0.6%	0-1%
Mo	0.34-0.40%	0-0.7%
Co	0.3-0.36%	N/A
W	0.13-0.2%	N/A

A comparison of the GEA of the stainless-steel capsule removed from the target and the activation products from the stainless-steel only in the fully assembled target is shown in Table 6-5. This includes a comparison between the first and last counts of the fully assembled target as well as the removed stainless-steel material. The stainless-steel capsule was analyzed by GEA 22 times in the full target assembly, and once as the isolated material. Due to the difficulties deconvoluting the ^{99}Mo, and ^{95}Zr, they are not included in Table 6-5.

Several nuclear reactions occurred to produce the activation products shown in Table 6-5, including ^{56}Fe(n,p)^{56}Mn, ^{58}Ni(n,2n)^{57}Ni to list a few. Due to the short analysis time after bombardment, short lived activation products such as ^{56}Mn was detectable, whose $t_{1/2}$ is 2.58 hours.

Table 6-5. Comparison of the GEA analysis of 14 MeV neutron activated stainless-steel capsule at first analysis, 100 day and isolated stainless-steel material. EOB: End of Bombardment.

		Full Assembly 1st count		Full Assembly 100-day count		SS alone	
EOB (d)		0.089		100.1		152.3	
	$t_{1/2}$ (d)	**Atoms/sample**	**%**	**Atoms/sample**	**%**	**Atoms/sample**	**%**
Cr-51	27.7	$8.5x10^{10}$	0.5	$6.4x10^{11}$	3.1	$1.7x10^{10}$	1.5
Mn-54	312.1	$3.7x10^{10}$	0.6			$7.1x10^{9}$	0.6
Mn-56	0.107	$8.7x10^{10}$	0.9	$3.6x10^{10}$	1.7		
Co-56	77.2					$1.0x10^{7}$	7.9
Fe-59	44.5	$2.1x10^{8}$	10.4			$3.5x10^{7}$	6.0
Ni-57	1.48	$2.3x10^{9}$	1.7				
Co-57	271.7	$2.8x10^{11}$	1.4	$6.2x10^{11}$	2.0	$8.9x10^{9}$	0.8
Co-58	70.9	$2.6x10^{10}$	0.4	$2.5x10^{10}$	1.5	$4.8x10^{9}$	0.6
Co-60	1955	$4.5x10^{9}$	13.1	$1.8x10^{9}$	87.0	$7.6x10^{8}$	1.1

6.2.2 Dissolved Pu Separation and Analysis

6.2.2.1 Pu in solution

TIMS analysis was used for confirmation of the Pu isotopic ratios. The raw percent of the total mass the percent relative to ^{239}Pu, a comparison between the historical values and the post irradiation values is included in Table 6-6. Of note is the percent reported for post irradiation, which is reported as the total Pu, while pre irradiation is the total target which should adjust the total percent a small amount to account for the full elemental composition

Table 6-6. Summary of TIMS analysis of Pu-3 target material before and after irradiation, reported in FY22 as the % mass relative to ^{239}Pu and the total Pu, the value reported from FY 16 is the % of the total mass including all trace elements, the bulk of the discrepancy is from the Ga included in the Pu metal.

	FY22 Post-irradiation		**FY16 Pre-Irradiation**
Isotope	**% X/^{239}Pu (2σ)**	**% of total Pu**	**% of total mass**
^{238}Pu	0.01151(3)	0.0108 (3)	0.011(3)
^{239}Pu	N/A	93.97	92.93(3)
^{240}Pu	6.102 (2)	5.734 (2)	5.73(3)
^{241}Pu/^{241}Am	0.253 (1)	0.238 (1)	0.263(1)
^{242}Pu	0.0511(1)	0.0480 (1)	0.0304(2)

Confirmation of the Pu isotopic distribution was performed using GEA, examining the primary gamma emissions from the various Pu isotopes. The results of this are shown in Table 6-7. The values for the percent composition of each of the Pu isotopes using GEA are in good agreement with that found by mass spectrometry. This analysis was dependent on the mass of the Pu in the A solution. In other words, the large mass allowed for the low branching ratio gamma emissions to be detected whereas this would have been more difficult in a small mass sample. To illustrate this point, in the target there was ~0.01-0.02% ^{238}Pu, analyzed using the largely interference free gamma emission at 152.7 keV whose branching ratio is 0.00093%, which allowed for the direct detection of the gamma signature of ^{238}Pu. There are higher branching ratio gamma emissions for ^{238}Pu, but these have significant interferences such as ^{241}Am (43.42 keV, 0.073%). [Soppera]

.

Table 6-7. GEA of Pu isotopes in the A solution. Uncertainty is 1σ including the propagated uncertainty determined from the instrument and branching ratio. For ^{239}Pu and ^{241}Pu the uncertainty is an assumed minimum uncertainty of 2%.

Isotope	Atoms/g	% of total Pu
^{238}Pu	$9.36 \times 10^{14} \pm 3.9\%$	0.010%
^{239}Pu	$8.97 \times 10^{18} \pm 2\%$	94.2%
^{240}Pu	$5.38 \times 10^{17} \pm 2.4\%$	5.70%
^{241}Pu	$5.18 \times 10^{15} \pm 2\%$	0.96%

6.2.2.2 Separated Fractions

The results from the separation efforts to remove the Pu from the samples solution, are shown in Figure 6-3. Results are the average of duplicate samples with associated 1σ uncertainty. Several the radionuclides were recovered in high yield (e.g., ^{95}Zr and ^{241}Am in the load and rinse fraction). The recovery of ^{95}Zr was significantly higher than 100%, reaching greater than 120% on average between the two replicates. It is expected that the bulk of radionuclides would not be retained by the anion exchange resin (due to their speciation in high molarity HNO_3). Several radionuclides are expected in the load rinse fraction such as the tracers ^{109}Cd, ^{111}Ag, ^{134}Cs, ^{152}Eu, and ^{237}Np (though the multiple Np oxidation states may cause issues). The bulk of the Pu (~50%) was eluted in the elute conditions as expected, combined with the second elution volume for a total of ~60-70% of the Pu recovered with some contaminants such as Ce, Np and Pa.

Due to the pandemic, a week transpired between the complete dissolution and the anion exchange loading. During this period, it is likely that changes in the speciation of the tracer metals lead to their unexpected elution behavior, i.e., ^{237}Np. To alleviate this issue, it is likely required to equilibrate the replicate solutions after the addition of the tracer solutions. This was not possible due to the required use of the glovebag and the materials within the bag.

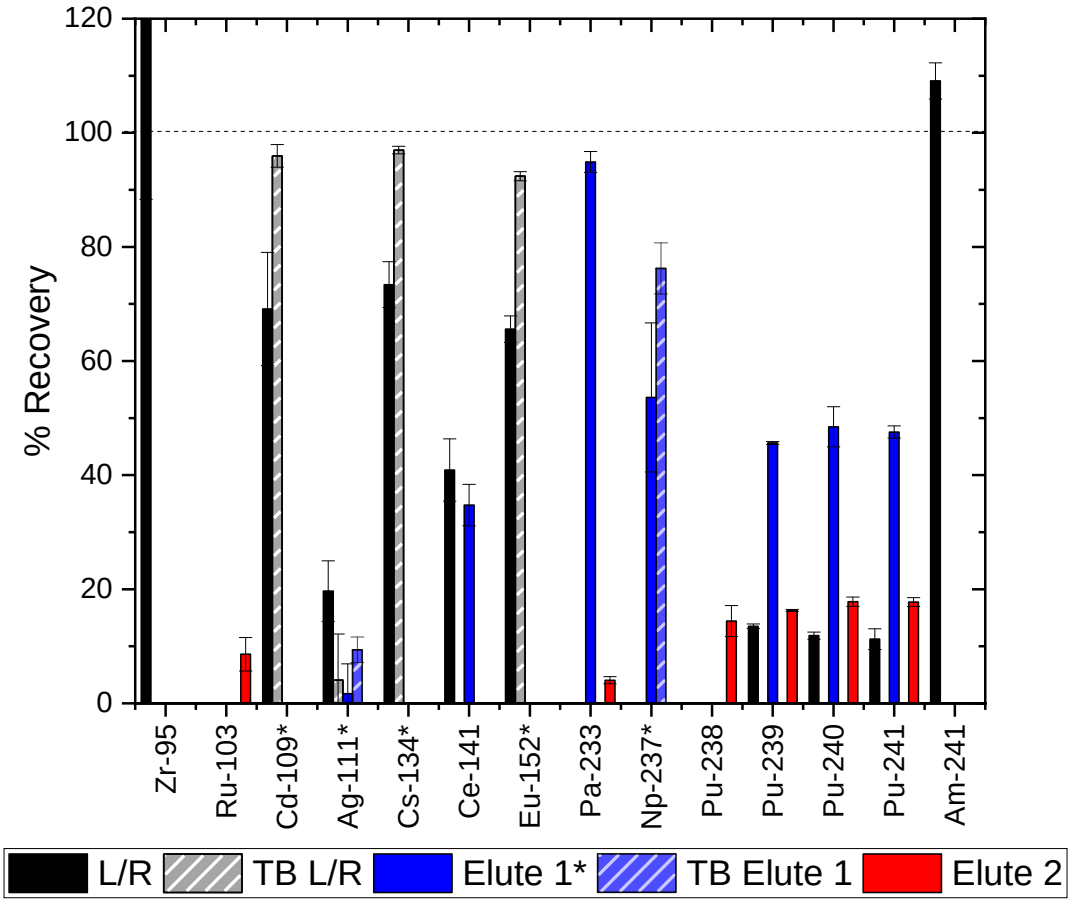

Figure 6-3. Analyzed fission products, tracers and actinides from separated Pu-3 target. Values presented for all except Elute 1, are the average of replicate measurements with 1σ of that value. Solid colored columns indicate the samples, lined columns indicate the tracer blanks.

7.0 Conclusion

PNNL performed an irradiation of 93% ^{239}Pu with 14 MeV neutrons followed, analyzing the resulting fission and activation products of the target assembly 22 times over 100 days using modern methods and instruments. Providing the first modern measurements of Pu fission at 14 MeV by a National Laboratory. The results from the fission product analysis were consistent with available literature for those fission products. The target was disassembled, and the Pu was dissolved as a demonstration for an upcoming joint experiment between Las Alamos National Laboratory (LANL) and PNNL in April 2022, irradiating the target at NCERC. The dissolution and subsequent separation demonstrated that the separation process could remove the Pu with little to no retention of the bulk of fission products. These results should provide foundational knowledge for the joint exercise. Though most of the fission products, and the results of the separation method agree well with literature, this work provides motivation for further analysis of fission at 14 MeV for ^{239}Pu.

8.0 References

Arrigo, LM; Friese, JF; Metz, LA. *Fabrication and Characterization of Plutonium Targets for Irradiation in the Flattop Critical Assembly.* PNNL-30265, Richland, WA.

2K v3.4.1 manual, Canberra Industries, Inc. www.canberra.com

England, TR; Rider, BF. “Evaluation and Compilation of Fission Product Yields. ENDF-349, LA-UR-94-3106, Los Alamos National Laboratory (1994), https://t2.lanl.gov/nis/publications/endf349.pdf

N. Soppera, M. Bossant, E. Dupont, "JANIS 4: An Improved Version of the NEA Java-based Nuclear Data Information System", Nuclear Data Sheets, Volume 120, June 2014, Pages 294-296

Appendix A PNNL Calculations and Associated Uncertainty

A.1 A solution GEA analysis

A.1.1 Atoms per gram A solution

Each A solution was analyzed by GEA multiple times and corrections were applied for decay during irradiation using the irradiation history of each measurement. The reported atoms per gram A solution (N/g A) for each isotope is the weighted average of the applicable counts using the formula shown in Equation 6; any counts which have interferences or very high uncertainty due to decay were discarded.

The uncertainty associated with the activity for each isotope in a GEA analysis is provided by the Genie 2k software and considers the counting statistics, the counting efficiency, and other applicable factors as described in the operator's manual. The weighted uncertainty for the average N/g A was calculated using Equations 7 and 8. The unweighted uncertainty for the average N/g A is calculated using the stdev.S function in Excel which uses the "n-1" method. The weighted and unweighted %RSD values were compared, and the higher value is reported which was typically the unweighted value. Example data is shown in Table 8-1.

$$\text{Average}_{\text{wtd}} = \frac{\frac{N_1}{\sigma_1^2} + \frac{N_2}{\sigma_2^2} + \frac{N_3}{\sigma_3^2}}{\frac{1}{\sigma_1^2} + \frac{1}{\sigma_2^2} + \frac{1}{\sigma_3^2}}$$

Equation 6

$$\sigma_{\text{wtd}} = \frac{1}{\frac{1}{\sigma_1^2} + \frac{1}{\sigma_2^2} + \frac{1}{\sigma_3^2}}$$

Equation 7

$$\%\text{RSD}_{\text{wtd}} = \frac{\sigma_{\text{wtd}}}{\text{Average}_{\text{wtd}}}$$

Equation 8

N is the atoms per gram of A solution
σ is the uncertainty
%RSD is the relative standard deviation
wtd is weighted

Table 8-1. Atoms per gram of A solution for Zr-97 in four A solution counts

	N/g A	± 1σ	$\%RSD_W$ (Weighted)	$\%\ RSD_U$ (Unweighted)
Count 1	$2.67x10^9$	$3.45x10^7$		
Count 2	$2.66x10^9$	$4.25x10^7$		
Count 3	$2.77x10^9$	$7.59x10^7$		
Count 4	$2.82x10^9$	$7.09x10^7$		
Weighted Average	$2.69x10^9$	$2.38x10^7$	± 0.883%	± 2.89%

A.1.2 R-value

The R-value was calculated using Equation 1 or Equation 2 which is repeated below in Equation 9 along with the applicable uncertainty shown in Equation 10.

$$R = \frac{\frac{N_X}{N_{Mo99}}}{r_{hist}} \text{ or } \frac{\frac{N_X}{N_{Mo99}}}{\left(\frac{CFY_X}{CFY_{Mo99}}\right)_{U235\ thermal}}$$

Equation 9

$$\sigma_R = \sqrt{\sigma_{N_X}^2 + \sigma_{N_{Mo99}}^2} \text{ or } \sqrt{\sigma_{N_X}^2 + \sigma_{N_{Mo99}}^2 + \sigma_{CFY_X}^2 + \sigma_{CFY_{Mo99}}^2}$$

Equation 10

The R-value and uncertainty are calculated in the same manner as given in Equations 9 and 10. The uncertainty for r_{hist} was not included. The uncertainty for values from ENDF/B-VIII.0 have been included if the uncertainty for the CFY is less than 64%; 64% propagates to an uncertainty of around 90% for the R-value which is rather meaningless and only impacts ^{91}Y, ^{93}Y, and ^{136}Cs.

If two replicates are found to have an average of $6.03x10^7$ ± 4.43% N/g A for ^{115}Cd and $4.08x10^8$ ± 2.15% N/g A for ^{99}Mo and the r_{hist} for ^{115}Cd is $2.07x10^{-3}$ then the R-value is 71.5 ± 4.93%.

$$R = \frac{\frac{6.03x10^7\ \text{N/g A solution } ^{115}\text{Cd}}{4.08x10^8\ \text{N/g A solution } ^{99}\text{Mo}}}{2.07x10^{-3}} = 71.5$$

$$\sigma_R = \sqrt{(4.43\%)^2 + (2.15\%)^2} = 4.93\%$$

A.2 Absolute Fission Yield Calculation Example

Equation 3 is repeated in Equation 11, with the intention of demonstrating its use in the calculation of the absolute fission yield for ^{136}Cs.

$$CFY_X = \frac{Atoms_X/g}{Fissions/g}$$

Equation 11

$$CFY_{Cs136thermal} = \frac{Atoms_{Cs136}/g}{Fissions/g} = \frac{2.04x10^8 \pm 3.7\%\ atoms/g}{3.53x10^{12} \pm 3.1\%\ fission/g} = 5.78x10^{-5} \pm 7.6\%$$

$$CFY_{Cs136fission} = \frac{Atoms_{Cs136}/g}{Fissions/g} = \frac{7.65x10^{6} \pm 2.0\%\ atoms/g}{5.97x10^{10} \pm 2.5\%\ fission/g} = 1.28x10^{-4} \pm 3.2\%$$

Relative Fission Yield Calculation Example

The R-value equation can be replaced with one containing only the CFYs for ^{99}Mo at different energies and the analyte of interest X as shown in Equation 12. The relative fission yield can then be calculated using by rearranging Equation 12.

$$\mathrm{R} = \frac{\left(\frac{CFY_X}{CFY_{Mo99}}\right)_{fission}}{\left(\frac{\mathrm{CFY_X}}{\mathrm{CFY_{Mo99}}}\right)_{\mathrm{U235\ thermal}}}$$

Equation 12

Rearrangement of Equation 12, the R-value used in the calculation of the relative fission yield is the average of all measured R-values for all fission spectrum campaigns that have been completed. The CFY used for thermal fission of ^{235}U for ^{136}Cs was calculated using the values measured from the FY21 thermal calibration campaign.

$$\mathrm{CFY}_{Xfission} = R \times \frac{CFY_{Mo99fission} \times CFY_{Xth}}{CFY_{Mo99th}}$$

Equation 13

$$\mathrm{CFY}_{136Csfission} = 2.29 \pm 4.1\% \times \frac{5.94x10^{-2} \pm 1.4\% \times 5.78x10^{-5} \pm 6.76\%}{6.11x10^{-2} \pm 1.4\%} = 1.36x10^{-4} \pm 8.1\%$$

A.1.3 Atoms per gram A solution

The analyte of interest in each replicate was converted from Bq/sample to a yield corrected N/g A solution as given in Equation 14 with the uncertainty given in Equation 15. Lambda is the decay constant for the given isotope.

$$\mathrm{N\ of\ X\ per\ g\ A} = \frac{\mathrm{Bq\ of\ X\ per\ separated\ fraction}}{\mathrm{mass\ of\ A\ solution}} * \frac{1}{\mathrm{Yield}} * \frac{1}{\mathrm{lambda\ of\ X}}$$

Equation 14

$$\mathrm{relative\ uncertainty\ (\%)} = \sigma_{\mathrm{rel}} = \sqrt{\sigma_1^2+\sigma_2^2+\ldots} = \sqrt{\sigma^2_{\mathrm{Bq\ of\ X}}+\sigma^2_{\mathrm{yield}}}$$

Equation 15

If a replicate containing 4.7134 g A solution was found to have 1.05x10^3 ± 1.50% Bq/sample ^{115}Cd and a yield of 97.7 ± 4.22% then the ^{115}Cd N/g A solution is 6.33x10^7 ± 4.47%.

$$\text{N/g A } ^{115}\text{Cd} = \frac{1.05\text{x}10^3 \text{ Bq/sample}}{4.7134 \text{ g A solution}} * \frac{1}{97.7\%} * \frac{1}{3.60\text{x}10^{-6}\text{s}^{-1}} = 6.33\text{x}10^7 \text{ N/g A solution}$$

$$\sigma_{\text{N/g A}} = \sqrt{(1.50\%)^2_{\text{Bq of X}} + (4.22\%)^2_{\text{yield}}} = 4.47\%$$

For samples with more than one replicate, the average N/g A solution was used for calculating the R-value for a given isotope. The uncertainty for the average is given in Equation 16 where S is the sample quantity (i.e., N/g A) and σ is the relative uncertainty for each S in %.

$$\sigma_{\text{ave}}\ (\%) = \frac{\sqrt{(S_1 * \sigma_1)^2 + (S_2 * \sigma_2)^2 + \ldots}}{\frac{S}{\sqrt{\#\text{ of reps}}}} * 100$$

Equation 16

If two replicates are found to have 6.33x10^7 ± 4.47% and 5.73x10^7 ± 4.37% N/g A solution ^{115}Cd, respectively, then the average is 6.03x10^7 ± 4.43% N/g A solution.

$$\sigma_{\text{ave}} = \frac{\sqrt{(6.33\text{x}10^7 * 4.47\%)^2 + (5.73\text{x}10^7 * 4.37\%)^2}}{\frac{6.03\text{x}10^7}{\sqrt{2}}} * 100 = 4.43\%$$

A.1.4 R-value

A.1.5 Atoms per fission

Activation products such as ^{237}U and ^{239}Np are reported in atoms per fission. The N/f and associated uncertainty is calculated in the same manner as given in Equation 9 and 2Equation 10.

$$\text{N of X per fission} = \text{N of X per g A} * \frac{1}{\text{fissions per g A}}$$

Equation 17

$$\text{relative uncertainty } (\%) = \sigma_{\text{rel}} = \sqrt{\sigma_1^2 + \sigma_2^2 + \ldots} = \sqrt{\sigma^2_{\text{N/g A}} + \sigma^2_{\text{f/g A}}}$$

Equation 18

If a replicate was found to have $1.46\text{x}10^{8}$ ± 3.16% N/g A ^{239}Np and $6.68\text{x}10^{9}$ ± 2.57% f/g A then the ^{239}Np N/f is $2.19\text{x}10^{-2}$ ± 4.07%.

$$\text{N/f}\ ^{239}\text{Np} = 1.46\text{x}10^{8}\ \text{N/g A} * \frac{1}{6.68\text{x}10^{9}\ \text{f/g A}} = 2.19\text{x}10^{-2}\ \text{N/f}$$

$$\sigma_{\text{N/f}} = \sqrt{(3.16\%)^{2}_{\text{N/g A}} + (2.57\%)^{2}_{\text{f/g A}}} = 4.07\%$$

Pacific Northwest National Laboratory

902 Battelle Boulevard
P.O. Box 999
Richland, WA 99354

1-888-375-PNNL (7665)

www.pnnl.gov